PCCP

PAPER

View Article Online
View Journal | View Issue

Cite this: *Phys. Chem. Chem. Phys.*, 2017, **19**, 21101

Linking hygroscopicity and the surface microstructure of model inorganic salts, simple and complex carbohydrates, and authentic sea spray aerosol particles†

Armando D. Estillore,[a] Holly S. Morris,[b] Victor W. Or,[a] Hansol D. Lee,[b] Michael R. Alves,[a] Meagan A. Marciano,[a] Olga Laskina,[b] Zhen Qin,[b] Alexei V. Tivanski*[b] and Vicki H. Grassian*[ac]

Received 16th June 2017,
Accepted 10th July 2017

DOI: 10.1039/c7cp04051b

rsc.li/pccp

Individual airborne sea spray aerosol (SSA) particles show diversity in their morphologies and water uptake properties that are highly dependent on the biological, chemical, and physical processes within the sea subsurface and the sea surface microlayer. In this study, hygroscopicity data for model systems of organic compounds of marine origin mixed with NaCl are compared to data for authentic SSA samples collected in an ocean–atmosphere facility providing insights into the SSA particle growth, phase transitions and interactions with water vapor in the atmosphere. In particular, we combine single particle morphology analyses using atomic force microscopy (AFM) with hygroscopic growth measurements in order to provide important insights into particle hygroscopicity and the surface microstructure. For model systems, a range of simple and complex carbohydrates were studied including glucose, maltose, sucrose, laminarin, sodium alginate, and lipopolysaccharides. The measured hygroscopic growth was compared with predictions from the Extended-Aerosol Inorganics Model (E-AIM). It is shown here that the E-AIM model describes well the deliquescence transition and hygroscopic growth at low mass ratios but not as well for high ratios, most likely due to a high organic volume fraction. AFM imaging reveals that the equilibrium morphology of these single-component organic particles is amorphous. When NaCl is mixed with the organics, the particles adopt a core–shell morphology with a cubic NaCl core and the organics forming a shell similar to what is observed for the authentic SSA samples. The observation of such core–shell morphologies is found to be highly dependent on the salt to organic ratio and varies depending on the nature and solubility of the organic component. Additionally, single particle organic volume fraction AFM analysis of NaCl : glucose and NaCl : laminarin mixtures shows that the ratio of salt to organics in solution does not correspond exactly for individual particles – showing diversity within the ensemble of particles produced even for a simple two component system.

Introduction

Covering a substantial area of the Earth's surface, the ocean serves as one of the main sources of particulate matter in the atmosphere. Sea spray aerosols (SSAs) are generated by breaking waves in marine environments and account for the largest atmospheric aerosol flux.[1] In particular, SSAs are known to directly affect climate by reflecting and absorbing solar radiation[2] and indirectly by acting as cloud condensation nuclei[3,4] and ice-nucleating particles.[5,6] A major recent advance in the understanding of SSAs comes from atmospheric observations and laboratory studies showing that SSA particles are composed of a mixture of inorganic salts and complex organic and biologically derived components.[7] The organic and biological components of SSAs are size dependent and are derived from the rich biological activity and complex chemical processes occurring in the ocean.[8–10] In addition, the sea surface microlayer (SSML), a nutrient and organic rich layer at the ocean–atmosphere interface, is critical to the air–sea exchange of gases, particles, and aerosols.[11] The SSML has different chemical, biological, and physical properties compared to the subsurface waters and

[a] *Department of Chemistry and Biochemistry, University of California San Diego, 3030 Urey Hall Addition, 9500 Gilman Dr, Mail Code: 0314, La Jolla, CA 92093, USA. E-mail: vhgrassian@ucsd.edu; Fax: +1-858-534-6255; Tel: +1-858-534-2499*

[b] *Department of Chemistry, University of Iowa, E272 Chemistry Building, Iowa City, IA 52242, USA. E-mail: alexei-tivanski@uiowa.edu; Fax: +1-319-335-1270; Tel: +1-319-384-3692*

[c] *Scripps Institution of Oceanography and Department of Nanoengineering, University of California, San Diego, La Jolla, CA 92093, USA*

† Electronic supplementary information (ESI) available. See DOI: 10.1039/c7cp04051b

it has a profound influence on the composition of aerosol particles as they escape across the interface. The SSML is a rich mixture of organic compounds such as fatty acids, fatty alcohols, sterols, carbohydrates, proteins and more complex colloids and aggregates exuded by phytoplankton such as lipopolysaccharides (LPSs).[11,12]

In the authentic samples collected from a pristine region of the Pacific Ocean, Gagosian and coworkers[13] detected alcohols, fatty acid salts and esters as specific tracers of ocean-derived organic compounds in atmospheric aerosols. The organic compounds include saccharides, fatty acids, and a few other organic classes.[13] Progress in analytical instrumentation[14,15] has allowed for further identification of specific compounds in ocean-derived particles, including high molecular weight, partially oxidized biological compounds like monosaccharides and polysaccharides, fatty acids and alcohols, amines, amino acids, organosulfates, and sulfonates.[7,10,16–26] Notably, SSA particles also serve as a means of transporting biological marine microorganisms from the sea to the atmosphere.[20,27] For example, Patterson and coworkers[28] detected the presence of microorganisms such as bacteria, diatoms, virus particles, and marine membrane vesicles in SSAs using cryogenic transmission electron microscopy (cryo-TEM).

The size-dependent composition and surface properties of atmospheric aerosol particles largely control their impact on climate by affecting their ability to take up water. Far removed from their source, airborne SSAs are exposed to changing relative humidity (RH). When particles are subjected to increasing RH, phase transitions such as deliquescence may occur where a crystalline particle takes up water to form an aqueous droplet. Deliquescence is a thermodynamically controlled process and occurs at a substance-specific RH and is accompanied by rapid particle growth. Efflorescence is the reverse process of deliquescence where an aqueous aerosol is exposed to a decreasing RH, and the aerosol particles crystallize. Between the deliquescence relative humidity (DRH) and efflorescence relative humidity (ERH) is a metastable region where, upon drying from above the DRH, particles can be crystalline, partially crystalline, or aqueous droplets.[29,30] As water is taken up, particles grow in size and increase their scattering and thus affect climate by the direct aerosol effect.[31,32] Understanding the hygroscopicity of the nascent SSA particles is particularly challenging because of the presence of organics formed by the rich biological activity of their source and will profoundly influence the cooling and warming at the top of the atmosphere.[33] These organics possess a wide range of molecular forms, solubility, surface activity, conformation and orientation that could potentially affect the physicochemical properties of SSAs.

In this paper, we focus on the water uptake growth factor, relative humidity values for the deliquescence and efflorescence phase transitions and the particle surface microstructure of molecular mimics of simple (glucose, maltose, sucrose) and complex sugars (laminarin, exopolymeric substance and LPS), as important biologically derived compounds from the breakdown of bacterial cell walls, and their mixtures with simple inorganic salts. The choice of sugars is guided by the types of organics detected during a 30 day campaign in the Scripps Institution of Oceanography called the 2014 Investigation into Marine Particles and Transfer Science (IMPACTS).[7,34] We also compare the results from these laboratory-generated model systems with nascent SSA samples collected during IMPACTS at different points during a phytoplankton bloom within a unique ocean–air facility.

Experimental methods

A. Chemicals and reagents

All of the chemicals used were purchased directly from the manufacturers, utilized without further purification, and included sodium chloride (NaCl), ≥99% Fischer Scientific; sodium bromide (NaBr), ≥99% Sigma-Aldrich; glucose, ≥99.0%, Sigma-Aldrich; maltose, Sigma-Aldrich; sucrose, ≥99%, Sigma-Aldrich; sodium alginate, Sigma-Aldrich; lipopolysaccharide (LPS) of *Escherichia coli* (*E. coli*) 0111:B4, Sigma-Aldrich; nonanoic acid, ≥99%, Sigma-Aldrich; laminarin, Alfa Aesar. Single component aerosol particles were generated from a 0.5 or 1% wt/v aqueous solution using ultrapure water prepared on site (Thermo, Barnsted EasyPure- II; ≥18.2 MΩ cm resistivity). Mixed NaCl–organic particles were prepared from solution containing 1.0 wt% NaCl and the desired wt% of organics.

B. Water uptake experiments using a hygroscopicity tandem differential mobility analyzer (HTDMA)

The water uptake measurements of the single component and binary mixtures were performed online using the Multi-Analysis Aerosol Reactor System (MAARS) described in detail previously.[35] All measurements were conducted under sub-saturated conditions (RH < 100%). A stream of polydisperse aerosol particles was generated from an atomizer (TSI Inc., Model 3062), and the particles passed through dual diffusion dryers in series to dry the particle to RH ≤ 5% before sampling and size selection. The dry particles then travel through a TSI ^{85}Kr charger (TSI Inc., Model 3077) to attain an equilibrium charge distribution. A monodisperse population of dry particles was generated by sending the particles to the first differential mobility analyzer (DMA1, TSI Inc., Model 3080) with mobility diameters of *ca.* 100 ± 1.80 nm. After size selection, the aerosol particles were flown to a hydration chamber where the particles were exposed and equilibrated to a defined RH. The aerosol particles grew (or shrank) in this chamber before they entered the second DMA (DMA2). The RH was adjusted by varying the ratio of wet and dry air controlled using a commercial dry air generator (Parker Balston, model 75-62). Multiple RH sensors were used to monitor the RH to within ±1% throughout the hydration chamber. After exiting the reaction chamber, the aerosol particles exposed to specific RH conditions (40 s) were directed to a scanning mobility particle sizer (SMPS) consisting of DMA2 (TSI, Inc., model 3080) and a condensation particle counter (CPC, TSI 3776) for the measurement of the humidified size distribution. The water vapor was supplied through a Nafion system to the DMA2 sheath air, in which the RH is controlled to be nearly equal to that of the RH of the hydration chamber. The RH in DMA2 is monitored at the DMA inlets of the sample and sheath air and

at the outlet of the sheath air to confirm and ensure the uniformity of the RH in the DMA2. The RH is changed stepwise, and the size distribution is measured when the RH stabilizes (typical wait time is 5–20 min). For all measurements, the sheath and sample flow rates of the two DMAs were 3.0 and 0.3 liters per minute, respectively. All HTDMA measurements were conducted during hydration and dehydration processes. For the hydration process, the dry particles exiting from DMA1 were exposed to a monotonically increasing RH in both the chamber and DMA2 sheath until the resulting change in the size was measured using the SMPS system. For the dehydration process, the RH in the chamber was first ramped up to RH $\leq$ 85% to fully deliquesce the particles before they are subjected to a drying process by monotonically lowering the RH in DMA2. This enables the efflorescence relative humidity (ERH) to be measured. Fig. S1 (see the ESI†) represents a typical example of size-selected monodisperse aerosol population undergoing homogeneous hygroscopic growth with no change for the standard deviation of the monodisperse distribution.

C. Atomic force microscopy (AFM) imaging and hygroscopicity measurements

Laboratory generated samples analyzed in this study were generated by atomizing solutions of model systems. These particles were collected using a micro-orifice uniform deposition impactor (MOUDI, MSP Corp. Model 125-R) by depositing on a silicon wafer (Ted Pella Inc., Part No. 16008) at stage 8 of the MOUDI, corresponding to particles with an aerodynamic diameter of 0.18–0.32 μm and a flow rate of 10 L min^{-1}. We scanned the samples using the nanoIR2 microscopy system (Anasys, Santa Barbara, CA, USA), with a scan rate of 0.5–1.0 Hz and spring constant of 13–77 N m^{-1} in tapping mode. AFM imaging of the laboratory generated aerosol particles was conducted at T = 298 K, RH ~20% and ambient pressure.

Nascent SSA particles were collected during 2014 Investigation into Marine Particles and Transfer Science (IMPACTS)[34] campaign for offline hygroscopicity measurements using AFM. Particles for the AFM study were collected *via* deposition of particles on hydrophobically coated silicon wafers (Ted Pella Inc., Part No. 16008)[36] at stage 6 of MOUDI with an aerodynamic diameter of 0.36–0.50 μm. The substrate deposited particles were placed in an AFM humidity cell chamber described in full detail elsewhere.[30,37] In this chamber the SSA particles were exposed to a monotonically increasing RH from RH = 5–80% by varying the ratio of dry and wet air. A molecular force probe 3D AFM (Asylum Research, Santa Barbara, CA) was used for water uptake studies at 298 K. Images were collected in AC mode using silicon nitride AFM probes (MikroMasch, Model CSC37) with a nominal spring constant of 0.35 N m^{-1} and a typical tip radius of curvature of 10 nm. Scan rates were between 1.0–1.3 Hz.

Modeling methods

Modeling of the water uptake properties of NaCl/organic mixtures was performed using the extended aerosol inorganics model (E-AIM).[38–40] The E-AIM can be used to predict the water content, particle volume and density of mixed aerosol particles over a wide range of humidity conditions. Combined with the UNIFAC (universal quasi-chemical functional group activity coefficients), the E-AIM can be applied to estimate the activity coefficient of multicomponent aerosol systems composed of inorganic and organic components in the aqueous phase. The activities of water and ions present in the aqueous aerosol are calculated using the Pitzer, Simonson, and Clegg equations.[41] The UNIFAC model is used to predict the water activity coefficients of aqueous organic compounds on the basis of the functional group contribution method. All calculations were performed using the E-AIM available online (http://www.aim.env.uea.ac.uk/aim/aim.php). Specifically, the E-AIM thermodynamic model III was used for modeling the NaCl/organic mixed particles. The number of moles for the inorganic and organic component was input into the model. The RH was varied from 10 to 95%, at a fixed temperature 298.15 K. These parameterized calculations provide insights into water uptake of mixed particles as a function of RH.

Results and discussion

A. Hygroscopicity of authentic SSA samples collected in an ocean–atmosphere facility

By bringing real-world chemical complexity into the laboratory, SSA particles were collected during a month-long IMPACTS 2014 experiment devoid of any environmental background.[34] The water uptake profile of these particles was then investigated on a single particle basis using the volume equivalent diameter derived from AFM measurements to quantify the growth factors (GFs).[30] We have previously established AFM as an accurate method to quantitatively determine the hygroscopic properties of the substrate deposited submicrometer sized aerosol particles highlighting the ability to distinguish the single particle morphology and hygroscopicity simultaneously for chemically complex atmospheric samples.[30] The particle types generated are dependent on the phytoplankton bloom in the bulk water, traced by the chlorophyll-*a* (chl-*a*) concentration. Specifically, particles collected at three campaign dates were analyzed: July 13th (low chl-*a* concentration, pre-bloom), July 17th (chl-*a* peak, bloom), July 21st (chl-*a* concentration decreased, post-bloom). Fig. 1 shows the results of authentic SSA particle growth following exposure to changing RH under subsaturated conditions. The water uptake properties show clear evidence of multiple particle types with distinct and variable hygroscopicity that vary depending on the day of the experiment. During the bloom indicated by the spike in the PM1 organic measured using an aerosol mass spectrometer (AMS) (July 17), aliphatic rich organics were enriched in submicrometer particles.[34] The net effect of these organics on the GF of the nascent SSA is evident as shown in Fig. 1A (green curve) where it is the lowest relative to the other dates analyzed. These data suggest that the particle contains less soluble organics and that the water uptake behavior is suppressed relative to pre-bloom particles (July 13). The relative decrease in the growth factor from July 13 to July 17 can be

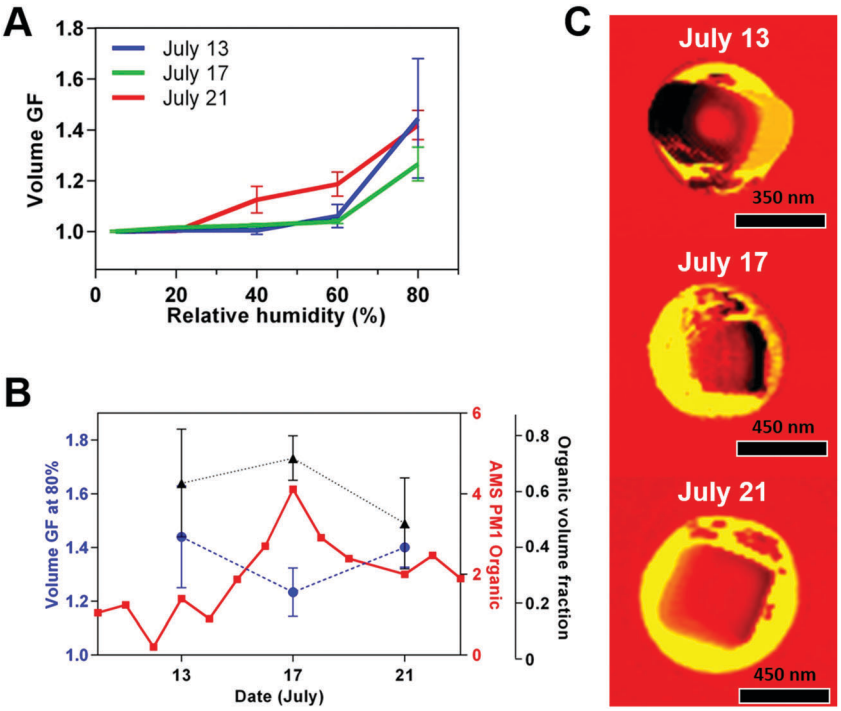

Fig. 1 (A) Hygroscopicity of the authentic SSA samples collected during the 2014 IMPACTS experiment measured by atomic force microscopy using the volume growth factor to calculate the growth factor and (B) correlation of the growth factor with the organic volume fraction of the nascent SSA particles. The aliphatic rich organics detected and measured by AMS shown in red peaked on July 17 corresponding to a peak in the organic volume fraction and suppressed GF. (C) AFM phase image of the authentic SSA particles collected during the 2014 IMPACTS experiment.

attributed to the increase in the organic to inorganic fraction, as evident from Fig. 1B organic volume fraction (OVF) data which can be calculated as:

$$\mathrm{OVF} = \frac{V_{\mathrm{particle}} - V_{\mathrm{core}}}{V_{\mathrm{particle}}} \quad (1)$$

where V_{particle} is the volume of the aerosol particle, V_{core} is the volume of the NaCl core.

Past the phytoplankton bloom (July 21), the GFs at 80% RH of the SSA particles are similar to July 13 even though there is a decrease in the OVF.[34] Fig. 1C shows the representative phase image of the authentic SSA particles collected during these three selected days, all showing a core–ring morphology. Furthermore, the particle growth profile of SSAs collected on Jul 21 showed an early uptake of water at RH $\sim$ 40%, which continues until the RH = 80%. This is indicative of more water-soluble organics such as carbohydrates (*e.g.* glucose) as supported by the GF for the model system studied as discussed in what follows and summarized in Table 1. The maximum in the OVF value and the corresponding depression of the GF on July 17 is highly corroborated with the trend of the values obtained with the model system shown in Table 1 which shows that an increase in the OVF results in a lower GF at RH = 80%.

As previously seen in field studies,[42–44] the reduction in the hygroscopicity of individual SSA particles highlights the role of organics in the interaction of individual atmospheric SSAs with water vapor. The variable responses of authentic SSA particles to water vapor underline the increasing level of chemical complexity[34,45] that can only be addressed in single particle-level studies that are otherwise obscured when probed using ensemble methods. As demonstrated in our model system studies detailed below, the degree of GF reduction is highly dependent on the

Table 1 Summary of deliquescence relative humidity, efflorescence relative humidity, growth factors, and hygroscopicity parameter (κ) at RH = 85% of substances and mixtures investigated in this work

Compound/mixture	Deliquescence relative humidity, %	Efflorescence relative humidity, %	Growth factor at RH = 85%	Hygroscopicity parameter, κ (RH = 85%)
NaCl	75.0 ± 0.50	44.0 ± 1.0	2.16 ± 0.04	1.27
NaBr	45.8 ± 0.70	17.0 ± 2.2	1.83 ± 0.06	1.01
NaCl : glucose (2 : 1)[a]	69.2 ± 1.5	40.3 ± 1.3	1.73 ± 0.03	0.80
NaCl : sodium alginate (2 : 1)[a]	72.4 ± 1.5	41.8 ± 1.7	1.65 ± 0.03	0.68
NaCl : LPS (1 : 1)[a]	70.4 ± 1.6	42.5 ± 1.2	1.51 ± 0.03	0.47
NaCl : nonanoic acid (1 : 1)[a]	72.3 ± 1.2	41.0 ± 1.5	1.86 ± 0.05	1.00

[a] Mass ratio of solution used to form 100 nm aerosol particles.

organic fraction, which comprises compounds covering a wide range of molecular forms and solubility.

B. Interactions of water vapor with crystalline salt particles: NaCl and NaBr; and simple carbohydrates: glucose, maltose, and sucrose

The water uptake profile of salt aerosol particles is typically characterized by their deliquescence (liquefaction of solid particle) and efflorescence (solidification of supersaturated solution) relative humidity. Fig. S2A (ESI†) shows the hygroscopic growth of NaCl as a function of RH as the test molecule for validating the MAARS system since its phase transition is known and its hygroscopicity has been well-studied using a variety of techniques. The NaCl particles imaged under ambient conditions (RH = 30%) using AFM show a cubic morphology as shown in Fig. S2C (ESI†). Upon increase of humidity, NaCl particles take up water to transition from a crystalline dry particle to an aqueous phase at a specific DRH of 75.5 ± 0.50%. AFM imaging conducted by Morris *et al.*[30] showed that as the RH was increased towards 75%, the salt particles start to become rounded. Beyond this RH, the solid NaCl particles become wet particles accompanied by a further increase in the growth factor. Spectroscopic studies by Ewing on the mechanism of H_2O–NaCl interactions showed that water not only physically adsorbs to the NaCl surface to form an adlayer but also dissociates on defect sites (*i.e.* steps, corners, edges, and vacancies) at the surface of NaCl.[46,47] Fig. S2B (ESI†) shows the water uptake properties of NaBr as a function of RH. The water uptake profile of NaBr particles is characterized by discrete phase transitions, similar to NaCl crystalline particles, characterized by a DRH value of 45.8 ± 0.70% and ERH at 17 ± 2.2%. The equilibrium morphology of crystalline NaBr is seen to be cubic like NaCl as shown in Fig. S2D (ESI†). The presence of steps and corners on the NaCl and NaBr single particle surfaces can be clearly observed in Fig. S2C and D (ESI†), respectively.

Nascent SSA samples collected during a recent large scale mesocosm experiment during the IMPACTS 2014 study have been shown to be enriched in carbohydrates.[7,26] Fig. 2A shows the measured hygroscopic growth curves of glucose, maltose, and sucrose as laboratory mimics to simple marine carbohydrates. Compared to NaCl and NaBr, sugar aerosol particles do not show distinct deliquescence and efflorescence transitions. Instead, the particles show gradual deliquescence associated with a continuous increase in the size upon hydration. This water uptake profile suggests that these organic aerosol particles readily absorb water even at low RH that leads to an increase in the aerosol volume as evidenced by the increase in the

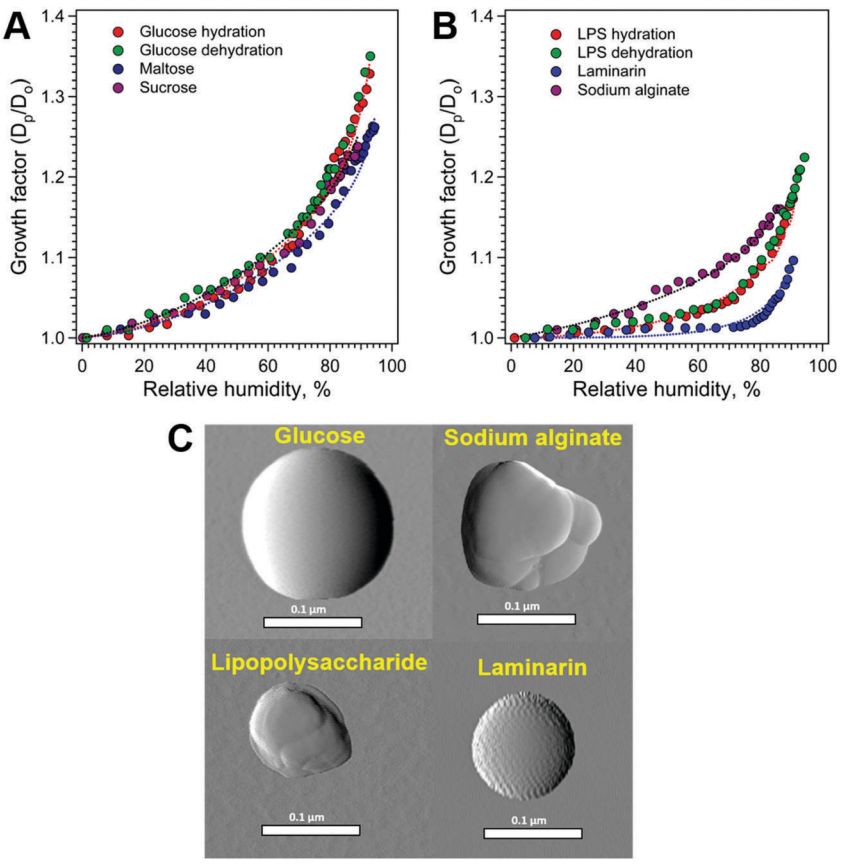

Fig. 2 Water uptake properties of D_0 = 100 nm of biologically-derived organic components of SSAs as a function of RH. (A) Simple sugars: glucose, maltose, and sucrose; and (B) complex sugars: laminarin and sodium alginate as the proxy for the exopolymeric substance, and lipopolysaccharides. (C) Amplitude AFM images of glucose, sodium alginate, lipopolysaccharide, and laminarin displaying different microstructures ranging from the amorphous rounded morphology (glucose and laminarin) to uneven and step surfaces (sodium alginate and lipopolysaccharide). Dotted lines are the fit to eqn (2).

growth factor. With decreasing RH, the aerosol particles slowly and readily lose their water content. This reversible uptake and release of water vapor without definite deliquescence and efflorescence has been observed in other organic aerosol particles such as compounds characteristic of biomass burning (levoglucosan and glucose)[48] and complex samples such as humic acids.[49,50]

The chemistry of sugars has been extensively studied in the food[51,52] and pharmaceutical[53] sciences showing compelling evidence of the propensity of sugars to form glasses, rubbers, gels, and ultra-viscous liquids with low molecular diffusivity. The presence of alcohol functional groups within sugars that can form hydrogen bonds with water results in swelling of the particles as the RH is increased. In addition, the morphology and phase state of particles can dictate their water uptake behavior.[54] To gain a better understanding of the nature of water uptake behavior of sugars, we perform imaging of the particles under ambient conditions using AFM, see Fig. 2C. Imaged glucose particles show a highly amorphous morphology and similar morphologies were also observed for maltose and sucrose particles. Amorphous substances have no long-range order and typically their water uptake profile proceeds through gradual water uptake where the transition from solid to liquid is nondiscrete.[55,56] Organic aerosol particles in the atmosphere can exist in an amorphous semi-solid or solid (*i.e.* glassy) state.[56] In these types of particles, bulk diffusion kinetics is important. Additionally, water accommodation and uptake occur at the outermost monolayers. Therefore, with increasing RH, the water acts as a plasticizer, which softens the matrix, thus reducing the viscosity and increasing the diffusion coefficient.[56] In addition, the continuous hygroscopic growth of amorphous substances usually involves several intermediate stages *via* the formation and swelling of gel-like structures in the highly concentrated aqueous sugar droplets, which is consistent with the tendency of sugar to form hydrogen bonds. In the atmosphere, diffusion of water into and within atmospheric aerosol droplets is important for various cloud formation processes. Zobrist *et al.*[57] showed that at low and atmospherically relevant temperatures ($T \leq 230$ K), organic constituents in aqueous aerosol particles can readily form glasses. Sucrose is known to display a glassy behavior under atmospherically relevant conditions in the RH range of 10–40%.[58] This has consequences for ice particle formation in cirrus clouds[59,60] or for secondary aerosol evolution.[61]

The growth factors of organics obtained from our HTDMA measurements can be fit to a parameterized function proposed by Dick *et al.*[62]

$$\mathrm{GF} = \left[1 + \left(a + b \cdot a_\mathrm{w} + c \cdot a_\mathrm{w}^2\right)\frac{a_\mathrm{w}}{1 - a_\mathrm{w}}\right]^{1/3} \qquad (2)$$

where a, b, and c are adjustable parameters and a_w is the water activity which is equal to RH(%)/100. The fitting parameters a, b, and c for carbohydrates studied in this work are summarized in Table S1 (ESI†). For glucose, the calculated growth at RH = 85% is 1.24 which is in excellent agreement with the GF determined by Mochida and Kawamura.[48]

C. Interactions of water vapor with complex carbohydrates: lipopolysaccharides (LPSs), sodium alginate and laminarin

LPSs consist of polysaccharide chains found on the surfaces of Gram-negative bacteria. They are classified as having three regions: a highly variable O-antigen region, a nonrepeating saccharide core, and a hydrophobic, membrane-anchoring domain known as lipid A.[63–65] LPSs, indicators of bacterial biomass, were previously detected and determined in the South China Sea and the Pacific Ocean.[66] Sodium alginate is used as a laboratory mimic for the extrapolymeric substance (EPS), a naturally occurring anionic polymer typically obtained from brown seaweed.[67] Alginate polymers are a family of linear unbranched polysaccharides which contain varying amounts of 1,4′-linked β-D-mannuronic acid and α-L-guluronic acid residues.[67]

There has been a study on the water uptake of protein macromolecules showing definite deliquescence and efflorescence. Mikhailov and coworkers[68] studied the hygroscopicity of protein bovine serum albumin (BSA) and mixtures of BSA with NaCl and NH_4NO_3 using HTDMA. Pure BSA particles exhibited deliquescence and efflorescence at RH = 35%. The experimental results obtained for pure sodium alginate, LPS, and laminarin particles with D_0 = 100 nm are illustrated in Fig. 2B showing a contrast behavior to BSA. There was no significant hysteresis between the measured particle diameters upon hydration and dehydration for EPS, LPS, and laminarin particles. Furthermore, the hygroscopic growth was much lower than that for inorganic salts. Specifically, the growth factor at RH = 85% is ~1.15 and ~1.12 for sodium alginate and LPS, respectively. Fig. 2A and B clearly demonstrates that chemical complexity has a profound effect on the GFs. This is directly supported by the comparison of simple and complex sugars. The GFs of complex sugars are lower compared to the simple sugars, as evident from the results shown in Fig. 2A and B.

One possible explanation for the continuous water accommodation of laminarin, EPS, and LPSs is the presence of physical defects of particles such as surface cracks, pores, and grain boundaries that has been previously explored experimentally.[69–71] These surface imperfections could facilitate and hasten the water adsorption and absorption processes even at low RH and retain water over the full RH range considered in this study. This is strongly supported by the AFM images of LPSs and sodium alginate showing uneven and step surfaces shown in Fig. 2C. Additionally, biopolymers are gelators known to form glasses similar to carbohydrates.[72] The individual macromolecules in polymeric substances can be entangled or cross-linked by covalent or H-bonds, van der Waals, or other types of interactions resulting in the formation of supramolecular networks exhibiting a rubbery state, which is evident from the amorphous rounded morphology displayed by laminarin particles shown in Fig. 2C.[73] The filling of water in surface imperfections leads to stepwise swelling of the particles during hydration resulting in a gradual deliquescence of the complex carbohydrate particles.

D. Interactions of water vapor with mixtures of sodium chloride and simple and complex carbohydrates

The abundance and composition of the organic mass fraction (0.17–0.83)[10,23] of SSAs are highly variable and are critically

linked to the complex biological, chemical, and physical processes occurring in the subsurface and surface ocean.[8,10,23,74] Ellison *et al.*,[75] suggested the "inverted micelle" concept where organic substances coat the sea-salt core. Depending on the chemical composition of the coatings, it can enhance or inhibit gas uptake and also affect the water uptake properties of aerosol particles.[76,77] Previous laboratory studies on the water uptake properties of mixed inorganic–organic compounds showed that the presence of soluble organic compounds can reduce the DRH of the mixture compared with single component inorganic particles.[78,79] On the other hand, highly insoluble long chain fatty acids such as palmitic acid, depending on the organic mass fraction, are found to have little to no effect on the deliquescence and efflorescence of inorganic crystalline salts.[80,81]

To determine the effect of simple and complex carbohydrates on the water uptake of crystalline aerosol particles, we probe the hygroscopicity of NaCl mixed with these carbohydrates at different atmospherically relevant mass ratios. The resulting water uptake profiles for the hydration of NaCl/glucose mixtures are shown in Fig. 3A along with the hydration curve of pure NaCl and pure glucose. The presence of water-soluble organic compounds showed an influence on the onset of deliquescence and efflorescence phase transition of the mixed aerosol particles as discussed in what follows. Relative to pure NaCl, the deliquescence of a 1 : 1 wt% mixture of NaCl and glucose is suppressed by ~3% RH and for a 1 : 2 wt% NaCl/glucose mixture the difference is ~8%. The GF at RH = 80% of the NaCl/glucose mixture is also marked by a decreasing trend with increasing glucose mass compared to the GF of pure NaCl but higher than that of pure glucose. At a 1 : 3 wt% NaCl/glucose mixture, the hydration curve completely lost its sharp phase transition and starts to display a behavior similar to that of pure glucose albeit at a higher GF at RH = 80%. The modeling results obtained using the E-AIM well describe the deliquescence transition and hygroscopic growth of NaCl/glucose mixed particles at 1 : 1 and 1 : 2 ratios of salt to organics as shown in the solid lines in Fig. 3A. At a 1 : 3 ratio as illustrated in the green curve, the water uptake profile of the mixed NaCl/glucose particles is not well-predicted using the model likely due to the high organic volume fraction where the glucose fully encapsulates the NaCl core as shown in Fig. 4A.

The resulting water uptake profiles of NaCl mixed with more complex sugars (laminarin) at different ratios are shown in Fig. 3B. At a 1 : 1 ratio, the DRH of the mixed particle is slightly lower than the DRH of pure NaCl and this value continues to shift to lower values with an increasing amount of laminarin. The water uptake profile of the mixed NaCl/laminarin loses the definite phase transition RH at a 1 : 5 mass ratio. Along with the changes in the DRH values there is the reduction of the GF in particles at RH = 80%. The results for NaCl/glucose and NaCl/laminarin at various salt to organic ratios are summarized in Table 2. The modeling results for the NaCl/laminarin mixture are shown in the solid lines in Fig. 3B. Similar to NaCl/glucose, the model predicts the phase transition for the 1 : 1, 1 : 2, and 1 : 3 ratios, albeit at a higher RH than the experiment. At a higher organic fraction (*i.e.* 1 : 4 and 1 : 5 ratios) where

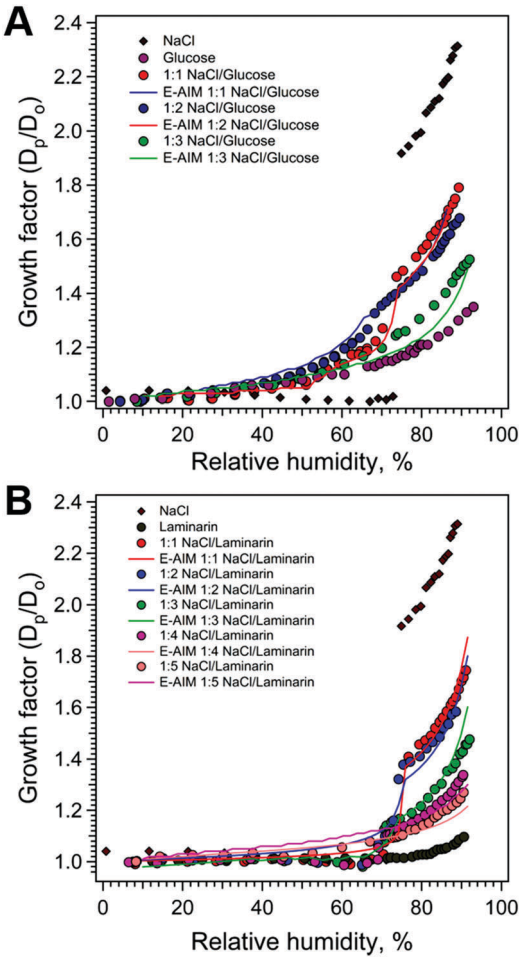

Fig. 3 Water uptake profiles of the 2-component mixture of (A) NaCl/glucose and (B) NaCl/laminarin at different mass ratios as a function of relative humidity. Water uptake profiles of pure NaCl, glucose and laminarin are also shown for comparison. Solid lines are based on the E-AIM model.

laminarin fully encapsulates the core as shown in Fig. 4B, the model under predicts the growth curve of the mixed NaCl/laminarin aerosol particles. These modeling results offer insights into the effects of simple and complex carbohydrates on the phase transitions of aerosol particles.

We next examined the morphology of these NaCl/carbohydrate mixtures. Understanding the morphology and microstructure of mixed inorganic/organic aerosol is important because the structure can influence the surface composition, the role of heterogeneous chemistry, gas–particle partitioning of semi volatile organics, and water uptake of aerosols in the sub- and supersaturated regimes.[82,83] Changes in RH can also induce separation of the organic and inorganic materials in individual atmospheric particles into distinct liquid phases.[84,85] Using AFM, we imaged the morphology of the mixed NaCl/organics considered in this study under ambient conditions. In the case of NaCl/glucose and NaCl/laminarin mixtures, shown in Fig. 4A and B respectively, the resulting particles adopt a spherical core–ring morphology with a well-defined NaCl core and the carbohydrates forming the ring. This is especially visible in the 1 : 1 NaCl/glucose ratio

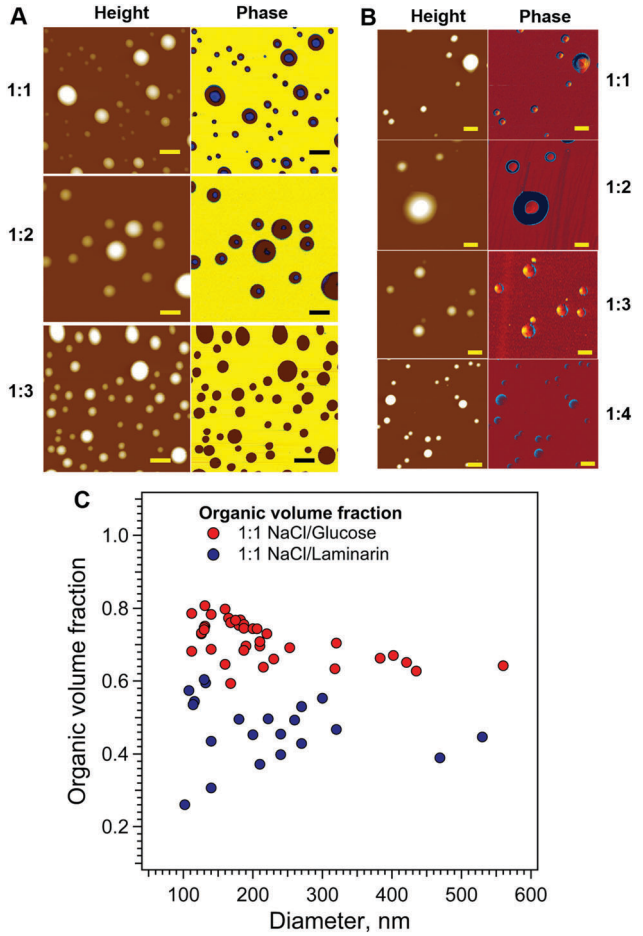

Fig. 4 Morphology of the 2-component mixture of (A) AFM height and phase images of the indicated NaCl/glucose mixture and (B) AFM height and phase images of the indicated NaCl/laminarin mixture at different mass ratios imaged under ambient conditions. (C) Comparison of the organic volume fraction for a 1 : 1 mass ratio of NaCl/glucose and NaCl/laminarin mixtures. Scale bar = 400 nm in (A) and (B).

shown in Fig. 4A (first row) for the height and phase images, respectively. Phase imaging enables mapping of surfaces based on the inorganic and organic components of aerosol particles. When these particles are exposed to elevated RH, water vapor first encounters the surface of the organic coating to effect dissolution or phase transition. As discussed above, the growth curves in pure organics are continuous and, therefore in the mixtures, continuous growth can be attributed to the continuous growth of the separate organic phase. In addition, these organics have the affinity for forming a strong network of hydrogen bonds with water molecules even at low RH and can delay the growth of particles and induce the inorganic components to be solubilized below their DRH, shifting the phase transitions to lower values compared to the pure inorganic component. The addition of NaCl can have a significant impact on the hydrogen bonding-network that these organics formed with water vapor because NaCl is recognized as "structure breakers," thus influencing the phase transitions of the mixed aerosol particles.[86] At a 1 : 2 NaCl/glucose ratio, the particles still show a core–ring morphology. However, the extent of glucose engulfing the NaCl core is much more pronounced showing less of the NaCl core as seen in Fig. 4A (second row) for the height and phase images, respectively. With a further increase in the glucose mass fraction, the resulting NaCl/glucose particles display an amorphous round shape similar to the pure glucose particles (see Fig. 2C). These particles show that the NaCl core is fully coated by the organic, as can be seen in the images shown in the last row of Fig. 4A. In the case of NaCl/laminarin mixtures (Fig. 4B), the particles also show a core–ring morphology for a 1 : 1, 1 : 2 and 1 : 3 mass ratio, which becomes amorphous round shaped particles without any clear NaCl core for higher amounts of organics. These results highlight the importance of the particle morphology and its impacts on the water uptake behavior of the aerosol particles. It is important to note that the "core–ring morphology" that the mixed particles adopt is highly dependent on the ratio of salt and organic components as illustrated by the AFM images obtained under ambient conditions.

It is noteworthy that it requires a smaller mass fraction of glucose to effectively suppress the sharp and defined deliquescence of NaCl compared to laminarin. This is due to the difference in the OVF when they are mixed with NaCl. This value can be calculated from eqn (1). The OVF analysis was conducted using Gwyddion software[87] and is based on the assumption that the core is inorganic and the shell is the

Table 2 Summary of organic volume fractions, deliquescence relative humidity, hygroscopicity parameter (κ at RH = 85%), and growth factors at RH = 60% and 80% of NaCl mixed with glucose and complex laminarin at various mass ratios

Mixture	Organic volume fraction	Deliquescence RH, %	Hygroscopicity parameter, κ (RH = 85%)	Growth factor	
				RH = 60%	RH = 80%
NaCl + glucose[a]					
1 : 1	0.71 ± 0.15	72.0 ± 2.0	0.68	1.14 ± 0.03	1.56 ± 0.02
1 : 2	0.85 ± 0.14	67.3 ± 2.0	0.57	1.20 ± 0.02	1.48 ± 0.03
1 : 3	—	Continuous	0.34	1.13 ± 0.02	1.24 ± 0.03
NaCl + laminarin[a]					
1 : 1	0.47 ± 0.21	73.8 ± 2.0	0.54	0.99 ± 0.04	1.51 ± 0.03
1 : 2	0.70 ± 0.15	73.0 ± 1.0	0.48	0.99 ± 0.03	1.44 ± 0.04
1 : 3	0.82 ± 0.14	70.6 ± 3.0	0.23	0.99 ± 0.04	1.22 ± 0.02
1 : 4	—	69.0 ± 3.0	0.18	0.99 ± 0.02	1.18 ± 0.05
1 : 5	—	Continuous	0.14	1.05 ± 0.02	1.14 ± 0.02

[a] Mass ratio of the solution used to form 100 nm aerosol particles.

organic component of the particle.[88] The calculated OVF as a function of particle size for the 1 : 1 mass ratios of NaCl/glucose and NaCl/laminarin is shown in Fig. 4C. For the same mass ratio, the OVF of NaCl/glucose (range 0.60–0.80) is higher compared to that of NaCl/laminarin (range 0.26–0.61). The higher OVF for the NaCl/glucose is in part due to the lower molar mass of glucose relative to laminarin, which contributes to the higher molar ratio of NaCl/Glucose for the same mass ratio. Furthermore, both systems display an increase in the OVF as the particle size decreases, which would result in a range of hygroscopic responses even for a simple 1 : 1 NaCl/organic mass ratio in solution. We note a greater amount of variation in the OVF in the 1 : 1 NaCl : organics mass mixture that involves less soluble laminarin relative to more soluble glucose. Such variation, even for a simple 1 : 1 mixture, will result in a range of hygroscopic behaviors when interrogated on a single particle level.[28] Table 2 summarizes OVFs and hygroscopicity parameter, κ at RH = 85% (see ESI† for details on calculating the hygroscopicity parameter) determined using AFM for NaCl : glucose and NaCl : laminarin at different mass ratios where a core–shell morphology was observed. The results demonstrate that the ratio of two compounds in solution does not correspond with that observed for the individual particles and depends on the nature and extent of solubility of the organic constituents. No values for the OVF are reported for the 1 : 3 NaCl/glucose and 1 : 4 and 1 : 5 NaCl/laminarin mass ratios because in these cases the organic fraction is sufficiently large such that the NaCl core cannot be uniquely identified from the AFM images.

The effects of mixing NaCl with other carbohydrates (LPS and sodium alginate) as well as nonanoic acid, a slightly soluble fatty acid, were also investigated and the water uptake profiles are shown in Fig. S3 (ESI†). Furthermore, Fig. S4 (ESI†) shows how the water uptake profiles change as a function of increasing the organic mass fraction for the NaCl/sodium alginate mixture, where a decrease in the GF and suppression of the deliquescence point are evident. The DRH and ERH of the binary mixtures studied are summarized in Table 1. Similar to the above, the presence of carbohydrates and other biological components of SSAs showed a significant influence on the physicochemical properties of SSAs. Table 2 summarizes the effects that include: depression of the overall particle diameter GF, a shift in the full deliquescence and efflorescence to lower RH values relative to pure NaCl, and with an increasing organic mass fraction the smoothing of hygroscopic GF is manifested.

Conclusions

A key property of SSAs that is relevant to the majority of aerosol impacts is their water uptake behavior. The contribution of organics to the hygroscopicity of SSAs has generally been neglected in air quality and climate models because of the challenges associated with the complexity of their chemical composition.[89] Although their morphology and biological functions can vary markedly, SSA particles play critical roles in modulating the interaction with solar radiation thus affecting global climate. A detailed knowledge on the dynamic structure, interactions with water vapor, and the specific roles that the organics play in cloud and ice formation, is imperative in bridging the gap of laboratory investigations and atmospheric observations. Here, we present the water properties of collected nascent SSA particles that exhibit diversity in their morphologies and water uptake properties that are highly dependent on the complex biological, chemical, and physical processes within the sea subsurface and the sea surface microlayer. Moreover, we also investigated the water uptake properties of marine relevant inorganic salts and marine derived biological compounds, in particular carbohydrates, detected in SSAs as single components and as mixtures with inorganic salts measured using a HTDMA.

Whereas sodium halides (NaCl and NaBr) clearly show sharp deliquescence and efflorescence, the growth curves of the organics are characterized by a continuous increase of the particle size as a function of RH demonstrating the hygroscopic nature of simple and complex carbohydrates even at low RH. This continuous and reversible water uptake behaviors of organics have important implications in their interaction with atmospheric oxidants. LPSs, for example, are shown to react towards atmospheric nitric acid.[64,65] Hygroscopic growth measurements of the inorganic–organics mixtures reveal that organics have an important influence on the growth factor and deliquescence of the inorganic salt. The water uptake GFs of the organics and NaCl/organic mixtures are lower relative to the inorganic salts. The DRH and ERH values of the salt–organics mixture are typically shifted to lower RH values compared to the inorganic components alone. The topography and morphology of the particles afforded by AFM imaging embody the microstructural information of the particles that reflects the underlying physicochemical properties of SSAs. The E-AIM results for the NaCl/organic mixed particles predict the deliquescence and hygroscopic growth for the simple system but failed for the complex system especially in the high organic fractions likely due to morphology effects. Our laboratory and field study results clearly show, in a consistent manner, the role that the organics play altering the evolving particle size of SSAs when subjected to RH cycling. The present study provides clear evidence that SSA is a complex mixture of organic and inorganic compounds and should not be considered as only a salt (*e.g.* NaCl).

Competing financial interest

The authors declare no competing financial interest.

Acknowledgements

We thank Prof. Christopher Cappa (UC Davis) for the insightful and helpful comments he provided. This work was supported by the National Science Foundation through the Centers of Chemical Innovation Program under Grant CHE1305427. The contents in this study do not necessarily reflect the official views of the National Science Foundation. The NSF does not endorse the purchase of the commercial products used in this report.

References

1 M. O. Andreae and D. Rosenfeld, *Earth-Sci. Rev.*, 2008, **89**, 13–41.
2 D. M. Murphy, J. R. Anderson, P. K. Quinn, L. M. McInnes and F. J. Brechtel, *et al.*, *Nature*, 1998, **392**, 62–65.
3 A. D. Clarke, S. R. Owens and J. Zhou, *J. Geophys. Res.: Atmos.*, 2006, **111**, D06202.
4 P. K. Quinn and T. S. Bates, *Nature*, 2011, **480**, 51–56.
5 P. J. DeMott, T. C. J. Hill, C. S. McCluskey, K. A. Prather and D. B. Collins, *et al.*, *Proc. Natl. Acad. Sci. U. S. A.*, 2016, **113**, 5797–5803.
6 T. W. Wilson, L. A. Ladino, P. A. Alpert, M. N. Breckels and I. M. Brooks, *et al.*, *Nature*, 2015, **525**, 234–238.
7 R. E. Cochran, O. Laskina, J. V. Trueblood, A. D. Estillore and H. S. Morris, *et al.*, *Chem.*, 2017, **2**, 655–667.
8 K. A. Prather, T. H. Bertram, V. H. Grassian, G. B. Deane and M. D. Stokes, *et al.*, *Proc. Natl. Acad. Sci. U. S. A.*, 2013, **110**, 7550–7555.
9 P. K. Quinn, D. B. Collins, V. H. Grassian, K. A. Prather and T. S. Bates, *Chem. Rev.*, 2015, **115**, 4383–4399.
10 C. D. O'Dowd, M. C. Facchini, F. Cavalli, D. Ceburnis and M. Mircea, *et al.*, *Nature*, 2004, **431**, 676–680.
11 D. J. Donaldson and C. George, *Environ. Sci. Technol.*, 2012, **46**, 10385–10389.
12 M. Cunliffe, A. Engel, S. Frka, B. Gašparović and C. Guitart, *et al.*, *Prog. Oceanogr.*, 2013, **109**, 104–116.
13 R. B. Gagosian, O. C. Zafiriou, E. T. Peltzer and J. B. Alford, *J. Geophys. Res.*, 1982, **87**, 11133–11144.
14 A. Laskin, M. K. Gilles, D. A. Knopf, B. Wang and S. China, *Annu. Rev. Anal. Chem.*, 2016, **9**, 117–143.
15 A. P. Ault and J. L. Axson, *Anal. Chem.*, 2017, **89**, 430–452.
16 M. Mochida, Y. Kitamori, K. Kawamura, Y. Nojiri and K. Suzuki, *J. Geophys. Res.: Atmos.*, 2002, **107**, D174325.
17 F. Cavalli, M. C. Facchini, S. Decesari, M. Mircea and L. Emblico, *et al.*, *J. Geophys. Res.: Atmos.*, 2004, **109**, D24215.
18 K. K. Crahan, D. A. Hegg, D. S. Covert, H. Jonsson and J. S. Reid, *et al.*, *J. Atmos. Sci.*, 2004, **61**, 2544–2558.
19 M.-A. Sicre and E. T. Peltzer, *Atmos. Environ.*, 2004, **38**, 1615–1624.
20 J. Y. Aller, M. R. Kuznetsova, C. J. Jahns and P. F. Kemp, *J. Aerosol Sci.*, 2005, **36**, 801–812.
21 M. Kuznetsova, C. Lee and J. Aller, *Mar. Chem.*, 2005, **96**, 359–377.
22 C. Leck and E. K. Bigg, *Geophys. Res. Lett.*, 2005, **32**, L19803–19804.
23 M. C. Facchini, M. Rinaldi, S. Decesari, C. Carbone and E. Finessi, *et al.*, *Geophys. Res. Lett.*, 2008, **35**, L17814.
24 R. E. Cochran, O. Laskina, T. Jayarathne, A. Laskin and J. Laskin, *et al.*, *Environ. Sci. Technol.*, 2016, **50**, 2477–2486.
25 L. N. Hawkins and L. M. Russell, *Adv. Meteorol.*, 2010, 612132.
26 T. Jayarathne, C. M. Sultana, C. Lee, F. Malfatti and J. L. Cox, *et al.*, *Environ. Sci. Technol.*, 2016, **50**, 11511–11520.
27 C. Leck and E. K. Bigg, *Tellus*, 2005, **57B**, 305–316.
28 J. P. Patterson, D. B. Collins, J. M. Michaud, J. L. Axson and C. M. Sultana, *et al.*, *ACS Cent. Sci.*, 2016, **2**, 40–47.
29 S. T. Martin, *Chem. Rev.*, 2000, **100**, 3403–3454.
30 H. S. Morris, A. D. Estillore, O. Laskina, V. H. Grassian and A. V. Tivanski, *Anal. Chem.*, 2016, **88**, 3647–3654.
31 D. K. Farmer, C. D. Cappa and S. M. Kreidenweis, *Chem. Rev.*, 2015, **115**, 4199–4217.
32 M. Tang, D. J. Cziczo and V. H. Grassian, *Chem. Rev.*, 2016, **116**, 4205–4259.
33 C. A. Randles, L. M. Russell and V. Ramaswamy, *Geophys. Res. Lett.*, 2004, **31**, L16108.
34 X. Wang, C. M. Sultana, J. Trueblood, T. C. J. Hill and F. Malfatti, *et al.*, *ACS Cent. Sci.*, 2015, **1**, 124–131.
35 E. R. Gibson, P. K. Hudson and V. H. Grassian, *J. Phys. Chem. A*, 2006, **110**, 11785–11799.
36 O. Laskina, H. S. Morris, J. R. Grandquist, A. D. Estillore and E. A. Stone, *et al.*, *Environ. Sci. Technol.*, 2015, **49**, 13447–13453.
37 J. Baltrusaitis and V. H. Grassian, *J. Phys. Chem. A*, 2012, **116**, 9001.
38 S. L. Clegg and P. Brimblecombe, *J. Phys. Chem. A*, 1998, **102**, 2155–2171.
39 S. L. Clegg, J. H. Seinfeld and P. Brimblecombe, *J. Aerosol Sci.*, 2001, **32**, 713–738.
40 A. S. Wexler and S. L. Clegg, *J. Geophys. Res.*, 2002, **107**, 4207.
41 S. L. Clegg, K. S. Pitzer and P. Brimblecombe, *J. Phys. Chem.*, 1992, **96**, 9470–9479.
42 S. D. Forestieri, G. C. Cornwell, T. M. Helgestad, K. A. Moore and C. Lee, *et al.*, *Atmos. Chem. Phys.*, 2016, **16**, 9003–9018.
43 A. Vaishya, J. Ovadnevaite, J. Bialek, S. G. Jennings and D. Ceburnis, *et al.*, *Geophys. Res. Lett.*, 2013, **40**, 6395–6398.
44 X. Zhang, P. Massoli, P. K. Quinn, T. S. Bates and C. D. Cappa, *J. Geophys. Res.: Atmos.*, 2014, **119**, 8384–8399.
45 H.-J. Eom, D. Gupta, H.-R. Cho, H. J. Hwang and S. D. Hur, *et al.*, *Atmos. Chem. Phys.*, 2016, **16**, 13823–13836.
46 D. J. Dai, S. J. Peters and G. E. Ewing, *J. Phys. Chem.*, 1995, **99**, 10299–10304.
47 M. C. Foster and G. E. Ewing, *J. Chem. Phys.*, 2000, **112**, 6817–6826.
48 M. Mochida and K. Kawamura, *J. Geophys. Res.*, 2004, **109**, D21202.
49 I. R. Zamora, A. Tabazadeh, D. M. Golden and M. Z. Jacobson, *J. Geophys. Res.*, 2011, **116**, D23207.
50 S. D. Brooks, P. J. DeMott and S. M. Kreidenweis, *Atmos. Environ.*, 2004, **38**, 1859–1868.
51 Y. Roos, *Carbohydr. Res.*, 1993, **238**, 39–48.
52 Y. H. Roos, *Annu. Rev. Food Sci. Technol.*, 2010, **1**, 469–496.
53 D. Q. M. Craig, P. G. Royall, V. L. Kett and M. L. Hopton, *Int. J. Pharm.*, 1999, **179**, 179–207.
54 N. Hodas, A. Zuend, W. Mui, R. C. Flagan and J. H. Seinfeld, *Atmos. Chem. Phys.*, 2015, **15**, 5027–5045.
55 E. Mikhailov, S. Vlasenko, S. T. Martin, T. Koop and U. Pöschl, *Atmos. Chem. Phys.*, 2009, **9**, 9491–9522.
56 T. Koop, J. Bookhold, M. Shiraiwa and U. Pöschl, *Phys. Chem. Chem. Phys.*, 2011, **13**, 19238–19255.
57 B. Zobrist, C. Marcolli, D. A. Pedernera and T. Koop, *Atmos. Chem. Phys.*, 2008, **8**, 5221–5244.
58 J. W. Lu, A. M. J. Rickards, J. S. Walker, K. J. Knox and R. E. H. Miles, *et al.*, *Phys. Chem. Chem. Phys.*, 2014, **16**, 9819–9830.

59 B. J. Murray, T. W. Wilson, S. Dobbie, Z. Cui and S. M. R. K. Al-Jumur, *et al.*, *Nat. Geosci.*, 2010, **3**, 233–237.
60 B. J. Murray, *Atmos. Chem. Phys.*, 2008, **8**, 5423–5433.
61 A. Virtanen, J. Joutsensaari, T. Koop, J. Kannosto and P. Yli-Pirilä, *et al.*, *Nature*, 2010, **467**, 824–827.
62 W. D. Dick, P. Saxena and P. H. McMurry, *J. Geophys. Res.*, 2000, **105**, 1471–1479.
63 C. R. H. Raetz and C. Whitfield, *Annu. Rev. Biochem.*, 2002, **71**, 635–700.
64 J. V. Trueblood, A. D. Estillore, C. Lee, J. A. Dowling and K. A. Prather, *et al.*, *J. Phys. Chem. A*, 2016, **120**, 6444–6450.
65 A. D. Estillore, J. V. Trueblood and V. H. Grassian, *Chem. Sci.*, 2016, **7**, 6604–6616.
66 M. Maeda, W. J. Lee and N. Taga, *Mar. Biol.*, 1983, **76**, 257–262.
67 K. Y. Lee and D. J. Mooney, *Prog. Polym. Sci.*, 2012, **37**, 106–126.
68 E. Mikhailov, S. Vlasenko, R. Niessner and U. Pöschl, *Atmos. Chem. Phys.*, 2004, **4**, 323–350.
69 A. A. Zardini, S. Sjogren, C. Marcolli, U. K. Krieger and M. Gysel, *et al.*, *Atmos. Chem. Phys.*, 2008, **8**, 5589–5601.
70 S. Sjogren, M. Gysel, E. Weingartner, U. Baltensperger and M. J. Cubison, *et al.*, *J. Aerosol Sci.*, 2007, **38**, 157–171.
71 E. Thomas, Y. Rudich, S. Trakhtenberg and R. Ussyshkin, *J. Geophys. Res.*, 1999, **104**, 16053–16059.
72 C. A. Angell, *Science*, 1995, **267**, 1924–1935.
73 L. A. Estroff and A. D. Hamilton, *Chem. Rev.*, 2004, **104**, 1201–1218.
74 L. M. Russell, L. N. Hawkins, A. A. Frossard, P. K. Quinn and T. S. Bates, *Proc. Natl. Acad. Sci. U. S. A.*, 2010, **107**, 6652–6657.
75 G. B. Ellison, A. F. Tuck and V. Vaida, *J. Geophys. Res.*, 1999, **104**, 11633–11641.
76 D. J. Donaldson and V. Vaida, *Chem. Rev.*, 2006, **106**, 1445–1461.
77 I. J. George and J. P. D. Abbatt, *Nat. Chem.*, 2010, **2**, 713–722.
78 P. Saxena, L. M. Hildemann, P. H. McMurry and J. H. Seinfeld, *J. Geophys. Res.: Atmos.*, 1995, **100**, 18755–18770.
79 M. Y. Choi and C. K. Chan, *Environ. Sci. Technol.*, 2002, **36**, 2422–2428.
80 R. M. Garland, M. E. Wise, M. R. Beaver, H. L. DeWitt and A. C. Aiken, *et al.*, *Atmos. Chem. Phys.*, 2005, **5**, 1951–1961.
81 M. E. Wise, K. J. Baustian and M. A. Tolbert, *Proc. Natl. Acad. Sci. U. S. A.*, 2010, **107**, 6693–6698.
82 N.-O. A. Kwamena, J. Buajarern and J. P. Reid, *J. Phys. Chem. A*, 2010, **114**, 5787–5795.
83 C. R. Ruehl, J. F. Davies and K. R. Wilson, *Science*, 2016, **351**, 1447–1450.
84 R. E. O'Brien, B. Wang, S. T. Kelly, N. Lundt and Y. You, *et al.*, *Environ. Sci. Technol.*, 2015, **49**, 4995–5002.
85 Y. You, L. Renbaum-Wolff, M. Carreras-Sospedra, S. J. Hanna and N. Hiranuma, *et al.*, *Proc. Natl. Acad. Sci. U. S. A.*, 2012, **109**, 13188–13193.
86 T. H. Lilley, in *Raman Spectroscopy of Aqueous Electrolyte Solutions*, ed. F. Franks, Plenum, New York, 1973, vol. 3, p. 265.
87 D. Nečas and P. Klapetek, *Cent. Eur. J. Phys.*, 2012, **10**, 181–188.
88 O. S. Ryder, N. R. Campbell, H. Morris, S. Forestieri and M. J. Ruppel, *et al.*, *J. Phys. Chem. A*, 2015, **119**, 11683–11692.
89 G. McFiggans, M. R. Alfarra, J. Allan, K. Bower and H. Coe, *et al.*, *Faraday Discuss.*, 2005, **130**, 341–362.